Inorganica Chimica Acta 362 (2009) 1323–1332

Contents lists available at ScienceDirect

Inorganica Chimica Acta

journal homepage: www.elsevier.com/locate/ica

# Studies of mononuclear and dinuclear complexes of dibromodimethylplatinum(IV): Preparation, characterization and crystal structures

Mairéad E. Kelly [a], Santiago Gómez-Ruiz [b], Ralph Kluge [a], Kurt Merzweiler [a], Dirk Steinborn [a], Christoph Wagner [a], Harry Schmidt [a,*]

[a] Institut für Chemie, Martin-Luther-Universität Halle-Wittenberg, Kurt-Mothes-Str. 2, 06120 Halle, Germany
[b] Departamento de Química Inorgánica y Analítica, Universidad Rey Juan Carlos, Móstoles 28933, Madrid, Spain

ARTICLE INFO

*Article history:*
Received 5 February 2008
Received in revised form 16 June 2008
Accepted 20 June 2008
Available online 27 June 2008

*Keywords:*
Dibromodimethylplatinum(IV)
Dinuclear complexes
X-ray crystal structures
*N*-donor heterocyclic ligands

ABSTRACT

A number of complexes of the types $[PtBr_2Me_2(N^{\frown}N)]$ ($N^{\frown}N$ = 4,4′-di-Me-2,2′-bpy (**1**); 4,4′-di-*t*-Bu-2,2′-bpy (**2**); 2,2′-bpz (**3**); bpym (**4**)) and $[PtBr_2Me_2(L)_2]$ (L = H-pz (**5**); 4-Me-H-pz (**6**); H-idz (**7**); H-im (**8**); H-bim (**9**); quaz (**10**)) are reported. Characterization by NMR ($^1H$, $^{13}C$ and $^{195}Pt$), IR and EI-MS is given. In addition, crystal structures of several of these complexes are described. Furthermore, interactions within these structures including intramolecular hydrogen bonding and π–π stacking interactions are reported. The reactivity of selected mononuclear complexes was investigated and yielded two dinuclear complexes $[PPh_4][(PtBrMe_2)_2(\mu\text{-}Br)(\mu\text{-}pz)_2]$ (**11**) and $[(PtBr_2Me_2)_2(\mu\text{-}bpym)]$ (**12**), respectively. The latter complex is accompanied by a solid-state structure. Finally, the thermal stability of all complexes is reported.



## 1. Introduction

A goal of our work was the preparation of multinuclear platinum(IV) complexes. As part of our investigations, we prepared a number of mononuclear complexes incorporating the $PtBr_2Me_2$ moiety. Ligand exchange reactions of platinum(IV) complexes, either organometallic or inorganic, with nitrogen donors generally result in stable complexes. The ability of such complexes to behave as antitumor agents has been demonstrated [1]. Organometallic platinum(IV) complexes obtained from the Pope cluster ($[(PtMe_3I)_4]$) and resulting in trimethylplatinum(IV) derivatives are prevalent in the literature. Complexes of dimethylplatinum(IV) are relatively sparse owing more than likely to the limited synthetic routes for the preparation of a suitable starting material. To date the reactivity of the polynuclear complex $[(PtBr_2Me_2)_n]$ with various donor ligands has been examined [2–4], although only two solid-state structures containing the $PtBr_2Me_2$ moiety in mononuclear complexes [5,6] and a small number of platinum(IV) bromo bridged complexes have been reported [7]. The preparation of dinuclear complexes with bridging pyrazolato ligands, including numerous group 8–10 organometallic complexes, has been widely reported [8–13].

Herein a new member of this series, $[PPh_4][(PtBrMe_2)_2(\mu\text{-}Br)(\mu\text{-}pz)_2]$ (**11**), and its solid-state structure, the first such dibromodimethylplatinum(IV) dinuclear structure of this type, is reported. The characterization of a second dinuclear complex, a neutral bipyrimidine bridged complex with two dibromodimethylplatinum(IV) centers, is also described. In addition, the preparation and characterization, including several solid-state structures, of several $[PtBr_2Me_2(N^{\frown}N)]$ and $[PtBr_2Me_2(L)_2]$ complexes ($N^{\frown}N$ is a chelating bidentate nitrogen donor ligand and L a monodentate nitrogen donor ligand) is reported here.

## 2. Results and discussion

### 2.1. Preparation

Compounds **1**–**10** were prepared by direct combination of a stoichiometric amount of the respective ligand with $[(PtBr_2Me_2)_n]$ as shown in Scheme 1, path A and B. The syntheses are similar to procedures described for complexes with chelating nitrogen donor ligands, such as $[PtBr_2Me_2(2,2'\text{-bpy})]$ [2], or other complexes of the generic type $[PtBr_2Me_2(L)_2]$, where L is monodentate donor ligand [14].

The attack of bidentate nitrogen donors (path A) breaks up the coordination polymer $[(PtBr_2Me_2)_n]$ yielding mononuclear complexes of the type $[PtBr_2Me_2(N^{\frown}N)]$ ($N^{\frown}N$ = 4,4′-di-Me-2,2′-bpy (**1**); 4,4′-di-*t*-Bu-2,2′-bpy (**2**); 2,2′-bpz (**3**); bpym (**4**)). Similarly, the reaction of monodentate nitrogen donor ligands with $[(PtBr_2Me_2)_n]$ (path B) led to complexes of the type $[PtBr_2Me_2(L)_2]$ where L = pyrazole (H-pz) (**5**); 4-methyl-pyrazole (4-Me-H-pz) (**6**); indazole (H-idz) (**7**); imidazole (H-im) (**8**); benzimidazole (H-bim) (**9**); quinazoline (quaz) (**10**). Complexes **1**–**10** are of moderate

* Corresponding author. Tel.: +34 5 5525726; fax: +34 5 5527028.
*E-mail address:* h.schmidt@chemie.uni_halle.de (H. Schmidt).

0020-1693/$ - see front matter © 2008 Elsevier B.V. All rights reserved.
doi:10.1016/j.ica.2008.06.025

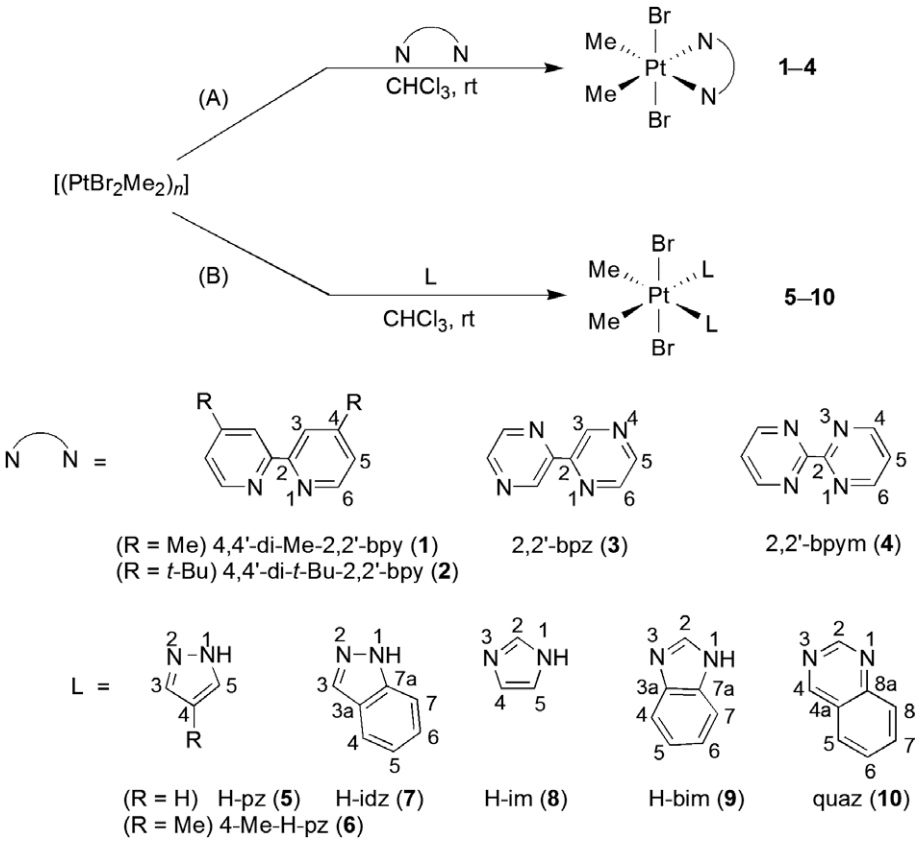


**Scheme 1.**

solubility in common organic solvents (methylene chloride, acetone) are air and moisture stable and were generally obtained in good to excellent yields, as shown in Table 1.

In addition, the homodinuclear complex $[PPh_4][(PtBrMe_2)_2(\mu\text{-}Br)(\mu\text{-}pz)_2]$ (**11**) was obtained, as illustrated by Scheme 2, on reaction of $[PtBr_2Me_2(H\text{-}pz)_2]$ (**5**) with stoichiometric amounts of KOH and $[(PtBr_2Me_2)_n]$ followed by the addition of $[PPh_4]Br$.

The dinuclear complex $[(PtBr_2Me_2)_2(\mu\text{-bpym})]$ (**12**) may be prepared by reacting $[PtBr_2Me_2(bpym)]$ (**4**) in chloroform with one equivalent of $[(PtBr_2Me_2)_n]$, as shown in Scheme 3, or by stirring $[(PtBr_2Me_2)_n]$ with half an equivalent of the bipyrimidine ligand.

Although complex **8**, $[PtBr_2Me_2(H\text{-}im)_2]$, was not possible to isolate in sufficient purity for full characterization the mononuclear complexes **1**–**7**, **9**, and **10** were characterized by NMR ($^1H$; $^{13}C$; $^{195}Pt$), EI-MS, IR, elemental analysis and, in some cases, by X-ray diffraction. Dinuclear complexes **11** and **12** were characterized by a combination of some of these techniques, as discussed below. Thermogravimetric monitored decomposition of **1**–**7** and **9**, respectively, generally appears to proceed *via* reductive elimination of MeBr. Complex **10** undergoes thermal decomposition with the initial elimination of $Br_2$. Fig. 1 shows the thermal decomposition of **7**. The percentage mass lost at $T_{dec}$ (176 °C) approximates to the mass of MeBr, thus indicating the formation of the platinum(II) complex $[PtBrMe(H\text{-}idz)_2]$. The dinuclear complexes **11** and **12** are significantly more thermally stable by ca. 40 K than their mononuclear starting complexes **5** and **4**, respectively. Complex **11** appears to decompose again with the elimination of MeBr but the mass loss observed for **12** is consistent with reductive elimination of $Br_2$.

**Table 1**
Summary of complexes isolated, the yield and decomposition temperatures

| Nr | Complex | Yield (%) | $T_{dec}$ (°C) |
|---|---|---|---|
| 1 | $[PtBr_2Me_2(4,4'\text{-di-Me-}2,2'\text{-bpy})]$ | 73 | 251–254 |
| 2 | $[PtBr_2Me_2(4,4'\text{-di-}t\text{-Bu-}2,2'\text{-bpy})]$ | 87 | 245–250 |
| 3 | $[PtBr_2Me_2(2,2'\text{-bpz})]$ | 94 | 198–201 |
| 4 | $[PtBr_2Me_2(bpym)]$ | 61 | 212–216 |
| 5 | $[PtBr_2Me_2(H\text{-}pz)_2]$ | 98 | 132–136 |
| 6 | $[PtBr_2Me_2(4\text{-Me-H-}pz)_2]$ | 74 | 127–132 |
| 7 | $[PtBr_2Me_2(H\text{-}idz)_2]$ | 100 | 176–180 |
| 8 | $[PtBr_2Me_2(H\text{-}im)_2]$ | 100[a] | [b] |
| 9 | $[PtBr_2Me_2(H\text{-}bim)_2]$ | 85 | 157–159 |
| 10 | $[PtBr_2Me_2(quaz)_2]$ | 45 | 160–163 |
| 11 | $[PPh_4][(PtBrMe_2)_2(\mu\text{-Br})(\mu\text{-}pz)_2]$ | 56 | 198–200 |
| 12 | $[(PtBr_2Me_2)_2(\mu\text{-bpym})]$ | 100 | 255–258 |

[a] Spectroscopic yield.
[b] Not determined.

## 2.2. Spectroscopic characterization

### 2.2.1. Mononuclear complexes *1*–*10*

Table 2 shows selected NMR data for both mononuclear (**1**–**10**) and dinuclear complexes (**11** and **12**).

Since only one set of signals assignable to the methyl ligands bonded to platinum is present in the respective $^1H$ and $^{13}C$ NMR spectra of **1**–**10**, it is clear that both methyl ligands are chemically equivalent. The magnitudes of the $^2J_{Pt,H}$ coupling constant (ca. 70–73 Hz) and the $CH_3$ chemical shift (1.79–2.21 ppm) indicate the *trans* configuration of nitrogen donor ligands to the methyl ligands. These findings are paralleled by $^1J_{Pt,C}$ couplings ranging from 501.4–529.9 Hz and Pt–$CH_3$ chemical shifts between −4.6 and −10.8 ppm. The values agree with those reported in the literature for similar complexes such as $[PtBr_2Me_2(py)_2]$ [3]. Thus, one isomer is formed in each reaction with the bromo ligands in the "axial" positions and the methyl and nitrogen donor ligands mutually *trans* configured in the "equatorial" plane (configuration index: *OC*–6–13).

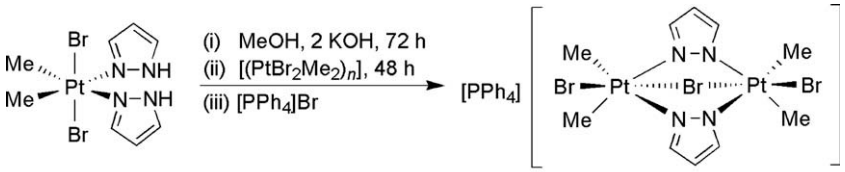


5 11

**Scheme 2.**

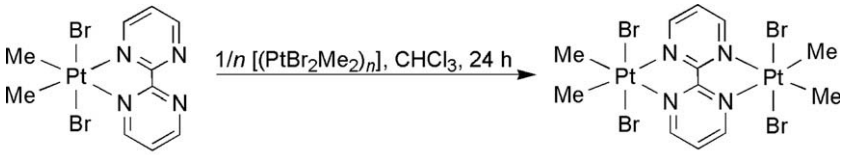


4 12

**Scheme 3.**

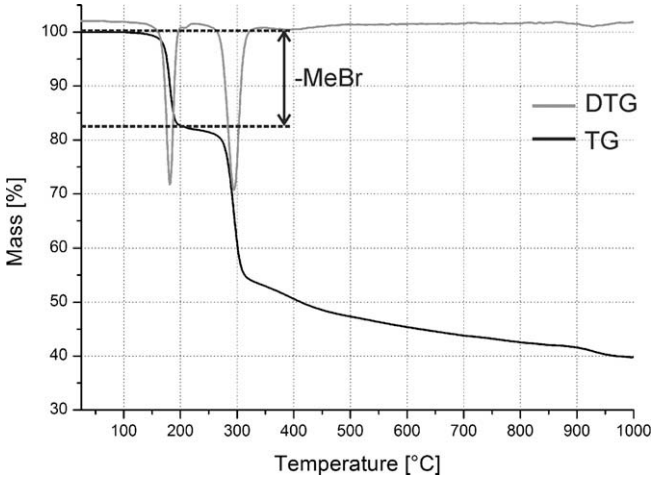


**Fig. 1.** Thermal decomposition of **7** as given by the thermogravimetric and differential thermogravimetric curves.

The signals arising from the aromatic nitrogen donor ligands of **1**–**10** have a downfield coordination induced shift of ca. 1 and 5 ppm in the $^{1}$H and $^{13}$C NMR spectra respectively. A summary of the chemical shift data for α-C–H to the coordinating nitrogen is given for **1**–**12** in Table 2. The chemical shift range of the resonances observed in the $^{195}$Pt NMR spectra of **1**–**10** between −2668 and −2308 ppm is consistent with values found for similarly configured platinum(IV) complexes [3]. The $^{195}$Pt NMR spectra of **1**–**4** ([$PtBr_2Me_2$(N⌒N)]) have $\delta_{Pt}$ values between −2668 and −2550 ppm, relative to a $H_2[PtCl_6]$ standard in $D_2O$ ($\delta$ 0 ppm). On the other hand, **5**–**10** ([$PtBr_2Me_2(L)_2$]) have shifts at lower field with $\delta_{Pt}$ varying between −2458 and −2308 ppm. This may be attributed to the "chelate ring effect" in **1**–**4** which results in an increased shielding of the platinum relative to similar complexes without chelate ligands [15,16].

EI-MS was possible for **1**–**7**. In general the formation of the molecular cationic radical is followed by fragmentation proceeding mainly *via* successive reductive elimination (neutral loss) of two MeBr. The distinctive isotopic pattern concurring with the presence of the $PtBr_2Me_2$ core and the corresponding ligand is found for the molecular cationic radical of each respective complex, as listed in Section 4.

### 2.2.2. Dinuclear complexes *11* and *12*

Both the $^{1}$H and $^{13}$C NMR spectra of [$PPh_4$][$(PtBrMe_2)_2$(μ-Br)(μ-pz)$_2$] (**11**) are consistent with the formation of one isomer in which bridging pyrazolato ligands (μ-pz) are *trans* configured to the methyl ligands and the bridging bromo ligand is *trans* configured to the terminal bromo ligands. The upfield shift of the methyl res-

**Table 2**
Selected $^{1}$H, $^{13}$C and $^{195}$Pt NMR data for mononuclear (**1**–**10**) and dinuclear (**11** and **12**) complexes

| Complex | Solvent | $\delta$(Pt–$CH_3$) ($^{2}J_{Pt,H}$) | $\delta$(Pt–$CH_3$) ($^{1}J_{Pt,C}$) | Aromatic Pt–N–$^{\alpha}$CH $\delta_H$; $\delta_C$ | $\delta_{Pt}$ |
|---|---|---|---|---|---|
| 1 | $CDCl_3$ | 2.11 (70.8) | −6.1 (518.6) | $C^6$H 8.75; 146.7 | −2550 |
| 2 | $CDCl_3$ | 2.12 (70.6) | −6.2 (515.7) | $C^6$H 8.74; 146.9 | −2556 |
| 3 | $CDCl_3$ | 2.21 (72.9) | −4.6[a] | $C^6$H 8.90; 141.2 | −2668 |
| 4 | $(D_3C)_2NCDO$ | 2.20 (72.8) | −5.9 (529.9) | $C^6$H 9.48; 155.6 | −2613 |
| 5 | $CDCl_3$ | 1.84 (72.4) | −10.4 (504.9) | $C^3$H 8.18; 139.2 | −2431 |
| 6 | $CDCl_3$ | 1.86 (72.2) | −10.8 (501.4) | $C^3$H 7.95; 139.2 | −2417 |
| 7 | $D_3COD$ | 1.79 (70.6) | −10.8 (506.7) | $C^3$H 8.77; 135.1 | −2340 |
| 8 | $CDCl_3$ | 2.04 (72.6) | −9.6 (502.9) | [b] | −2458 |
| 9 | $(D_3C)_2CO$ | 2.16 (71.4) | −8.1 (517.8) | $C^2$H 8.56; 146.0 | −2308 |
| 10 | $CDCl_3$ | 2.21 (71.8) | −7.8 | $C^4H$ 9.96[b]; $C^2H$ 9.55[b] | −2413 |
| 11 | $CDCl_3$ | 1.72 (66.6) | −12.6 | $C^{3/5}$H 7.58; 136.8 | −2287 |
| 12[c] | $(D_3C)_2NCDO$ | 2.25 (74.7) | [d] | $C^{4/6}$H 9.90[d] | −2618 |

Chemical shifts: (ppm); couplings in brackets: (Hz).
[a] Not observed.
[b] Assignment of carbon atom not possible.
[c] Data presented are those assigned to **12** in the presence of degradation products (see text).
[d] Solubility insufficient for acquisition.

onance in $^1$H NMR spectrum by approximately 0.2 ppm relative to that of **5** and the decrease in magnitude of the $^2J_{Pt,H}$ coupling (**5**/**11**: 72.4/66.6 Hz) is in accord with values previously reported for pyrazolato bridged complexes and illustrates the stronger *trans* influence of the pyrazolato ligand relative to the neutral pyrazole ligand [8]. The substantial upfield shift of C$^4$*H* (**5**/**11**: 6.37/5.83 ppm) and the equivalence of C$^3$*H* and C$^5$*H* (α-C–H to coordinated nitrogen atoms) in the $^1$H NMR spectrum of **11** also agree with the bridging mode of the pyrazolato ligand and $C_s$ molecular point group symmetry in solution. The same trend in resonance shift relative to **5** was also observed in $^{13}$C NMR spectrum of **11**. In the $^{195}$Pt NMR spectrum of **11** the equivalence of the platinum atoms is verified by the presence of one resonance at $\delta_{Pt}$ −2287 ppm, approximately 144 ppm downfield from the signal observed for **5**. The negative mode ESI-MS spectrum of compound **11** shows the presence of the anion $[C_{10}H_{18}Br_3N_4Pt_2]^-$ and the isotopic pattern is in good agreement with the calculated pattern for an anion of this elemental composition, as shown in Fig. 2. The spectrum in the positive mode shows the tetraphenylphosphonium cation.

The complex [(PtBr$_2$Me$_2$)$_2$(μ-bpym)] (**12**) was found to be too insoluble in most common organic solvents such as methanol, chloroform and nitromethane to obtain NMR spectra. The $^1$H NMR spectrum of the dinuclear **12** in DMF-$d_7$ contains three sets of signals arising from the dinuclear complex itself (60%) and equal amounts of each [PtBr$_2$Me$_2$(bpym)] **4** (20%) and [PtBr$_2$Me$_2$(DMF-$d_7$)$_2$] (20%) which results from solvation of [(PtBr$_2$Me$_2$)$_n$] in DMF-$d_7$ [2]. Scheme 4 illustrates the process yielding **4** and [PtBr$_2$Me$_2$(DMF-$d_7$)$_2$] from **12** in solution, as monitored by $^1$H NMR.

Fig. 3 shows the aromatic region of the spectrum in DMF-$d_7$ of the free ligand (spin system A$_2$X), **4** (ABX) and the dinuclear complex **12** (A$_2$X). The increased symmetry in going from **4** to **12** (ABX to A$_2$X) verifies the formation of dinuclear **12** with $D_{2h}$ molecular symmetry in solution. As described above for the mononuclear **1**–**10**, the proton resonances of the ligand are gradually shifted downfield in going from the free ligand to the chelating mode of **4** to the bridging mode of **12**.

Although the low solubility of **12** and the presence of multiple components in DMF-$d_7$ prevented acquisition of satisfactory $^{13}$C NMR data, it was possible to obtain a spectrum of the mixture in $^{195}$Pt NMR. The observation of three signals confirms the presence of the three platinum species in solution as depicted in Scheme 3, 12: $\delta_{Pt}$ −2618 ppm; **4**: $\delta_{Pt}$ −2613 ppm; [PtBr$_2$Me$_2$(DMF-$d_7$)$_2$]: $\delta_{Pt}$ −1892 ppm. The most highfield shifted resonance assignable to **12** is shifted just 5 ppm relative to the signal of **4**, indicating the similarity of their coordination environment. Negative mode ESI-MS of **12** in MeOH shows the presence of the anionic methoxy $[M+OCH_3]^-$ adduct. In the positive mode ESI-MS spectrum the sodium adduct $[M+Na]^+$ is found. The isotopic patterns emerging in both modes are satisfactory fits to the expected respective isotopic patterns (see Section 4). In addition, microanalysis of the powder isolated from the reaction is consistent with the formation of **12** only.

There is a significant amount of literature dealing with the assignment of IR spectra of dinuclear complexes with bridging bipyrimidine ligands [17–19]. The IR spectra of mononuclear **4** and dinuclear **12** show marked differences for the imine C=N stretching vibration. The spectrum of **4** has two absorptions at 1555 and 1573 cm$^{-1}$ while the spectrum of **12** contains only one absorption band assignable to the aromatic imine C=N stretching vibration at 1576 cm$^{-1}$, as may be expected for the symmetrical dinuclear complex **12**.

### 2.3. Single crystal studies

#### 2.3.1. Structures of mononuclear complexes *2*, *5*–*7* and *10*

Single crystals suitable for X-ray diffraction analysis were obtained for the mononuclear complexes **2**, **5**–**7** and **10**. Selected bond lengths and angles are given in Table 3.

All these complexes crystallize in discrete molecules with an approximate octahedral arrangement of the ligator atoms around the platinum. Complex **2** has molecular point group symmetry $C_s$ and complexes **6**, **7** and **10** have crystallographically imposed $C_2$ symmetry. In accord with the NMR spectroscopic results all complexes exhibit two bromo ligands in mutual *trans* position and two methyl ligands *trans* to the *N*-donor atoms. Due to the bite of the bpy ligand in **2** (Fig. 4), the N–Pt–N′ angle (75.2(3)°) is significantly smaller than 90°. All X–Pt–X′ angles (X, X′ = Br, C, N) between *cis* standing ligands in the complexes with monodentately bound *N*-donor ligands (Figs. 5 and 6, **5**–**7** and **10**) are between 86.8(6)° and 92.6(1)°.

In complexes **2**, **5**–**7** and **10** the Pt–C bonds (2.035(4)–2.081(7) Å), the Pt–N bonds (2.170(3)–2.206(9) Å) and the Pt–Br bonds (2.445(7)–2.47(1) Å) are in the expected range [20]. The angle between the least-square plane of the bpy ligand and the [PtC$_2$N$_2$] plane in **2** (Fig. 4) is 4.8(2)°. The interplanar angles γ between the least-squares planes of the monodentately bound *N*-heterocyclic ligands and the [PtC$_2$N$_2$] coordination plane are 43.2(3)–

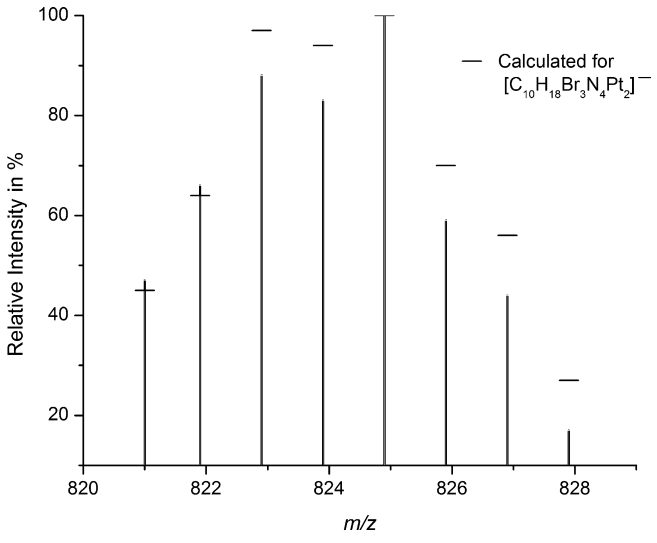


**Fig. 2.** Isotopic pattern of $[C_{10}H_{18}Br_3N_4Pt_2]^-$ from the negative mode ESI-MS spectrum of **11**. Calculated intensities are indicated by horizontal lines.

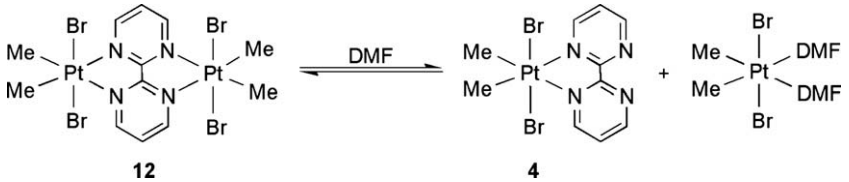


**Scheme 4.**

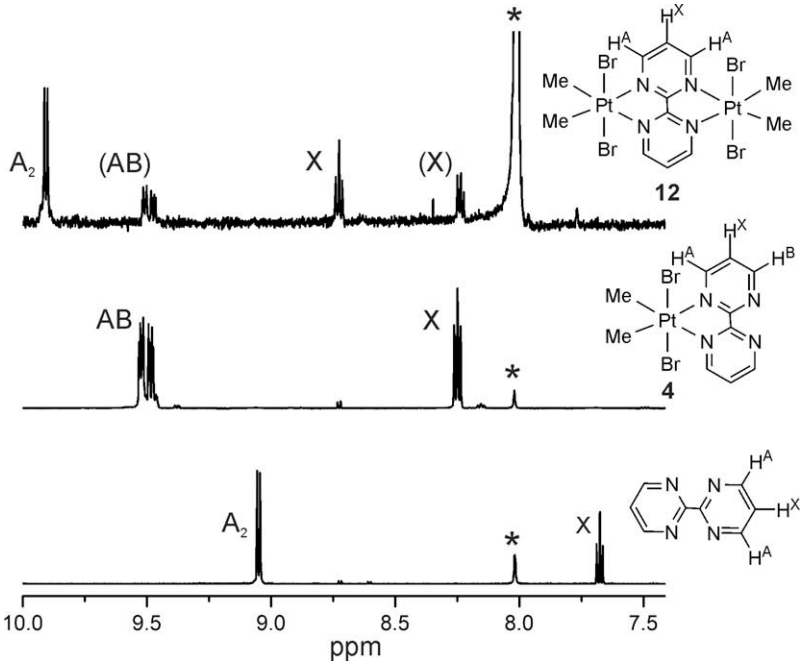


**Fig. 3.** Comparison of aromatic region from the $^1$H NMR spectra of dinuclear **12** ($A_2X$ spin system), mononuclear **4** (ABX) and the free bipyrimidine ligand ($A_2X$), all measured in DMF-$d_7$. *Solvent.

**Table 3**
Selected bond distances (in Å) and angles (in °) of **2**, **5**, **6**, **7** and **10**

| | **2** | **5** | **6** | **7** | **10** |
|---|---|---|---|---|---|
| Pt–C | 2.081(7) | 2.06(1)<br>2.06(1) | 2.035(4) | 2.043(9) | 2.042(6) |
| Pt–N | 2.172(6) | 2.19(1)<br>2.206(9) | 2.170(3) | 2.182(7) | 2.204(5) |
| Pt–Br | 2.452(1) 2.450(1) | 2.47(1)<br>2.453(2) | 2.452(1) | 2.457(1) | 2.445(7) |
| C–Pt–N | 173.8(3) | 178.4(5)<br>179.1(5) | 178.7(2) | 177.6(3) | 178.1(2) |
| N–Pt–N | 75.2(3) | 90.9(4) | 88.4(2) | 90.2(3) | 88.6(2) |
| Br–Pt–Br | 178.1(5) | 178.5(1) | 179.9(1) | 178.8(1) | 177.0(1) |
| $\gamma$[a] | | 79.4(7)<br>65.9(6) | 56.9(2) | 43.2(3) | 49.1(4) |

[a] Interplanar angle between the least-squares plane of the monodentately bound aromatic ligand and [$PtC_2N_2$] plane.

56.9(2)° for **6**, **7** and **10** but 79.4(7)° and 65.9(6)° for **5**, as shown in Table 3. Most of these interplanar angles are in the range reported for Pt(II) and Pt(IV) complexes having non-bridging non-chelating six-membered heterocyclic nitrogen donor ligands (median 39.9°; lower/upper quartile 29.3/45.2°; $n = 15$; $n$ = number of observations) [21].

Intramolecular N–H···Br hydrogen bonds (Table 4) in **5** and **6** indicated by N···Br distances less than the sum of the van der Waals radii (3.40 Å) were identified [22]. Although the values must not be overestimated due to calculated hydrogen atom positions the N–H···Br angles were also found to be in the expected range [23].

In crystals of the complexes 5, 7 and 10 weak intermolecular forces govern the molecular packing. In crystals of 5 the pyrazole rings bound via N1 of two neighboring molecules are π–π interacting (Fig. 7). The geometrical parameters (interplanar distance: 3.22 Å; centroid···centroid distance 3.60(1) Å; displacement angle[1] 24.7°) are in the range typical for such interactions [24]. Furthermore, the C3–H bonds of these rings interact with the pyrazole rings bound via N3 of the neighboring molecules in an edge-to-face

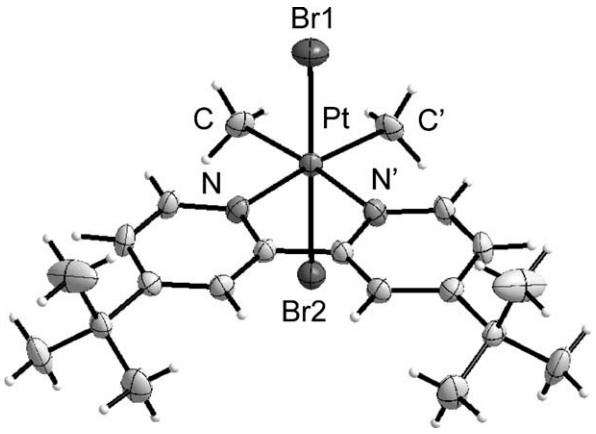


**Fig. 4.** Molecular structure of **2**. Displacement ellipsoids at 30% probability.

[1] Displacement angle: Angle between the vector connecting the centroids and normal to the plane of the ring.

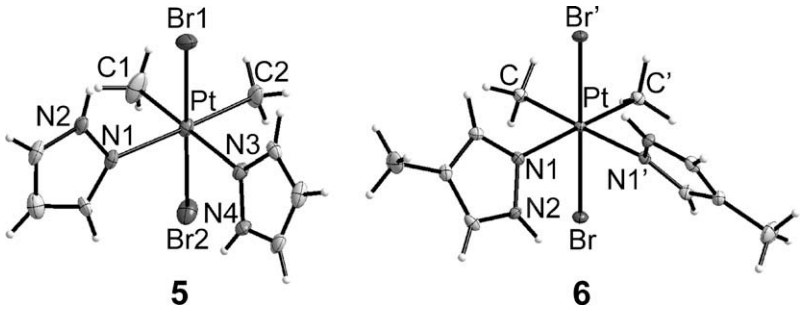


**Fig. 5.** Molecular structures of **5** and **6**. Displacement ellipsoids at 30% probability.

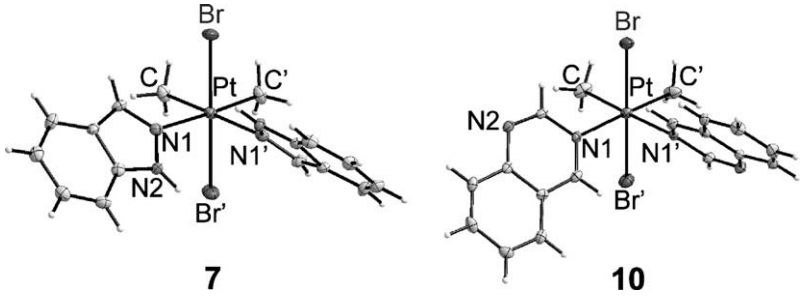


**Fig. 6.** Molecular structures of **7** and **10**. Displacement ellipsoids at 30% probability.

**Table 4**
Summary of parameters (distances in Å, angles in °) in crystals of **5**–**7** indicating weak hydrogen bonding interactions

| Complex | N···Br | | N–H···Br[a] | |
|---|---|---|---|---|
| 5 | N2···Br1 | 3.23(1) | N2–H···Br1 | 125 |
| | N4···Br2 | 3.32(1) | N4–H···Br2 | 117 |
| 6 | N2···Br | 3.30(1) | N2–H···Br | 113 |
| 7 | N2···Br | 3.38(1) | N2–H···Br | 146 |

[a] Based on calculated positions of hydrogen atoms.

(C–H···π type) interaction. The geometrical parameters (C3···centroid distance 3.460(1) Å; estimate C3–H8···centroid angle 155.0°) are in the expected range [24].

Similarly, π–π interactions are found between the respective aromatic ligands in crystals of **7** and **10**, as shown for **7** in Fig. 8a. Due to a crystallographic inversion center the indazole (**7**) and quinazoline (**10**) rings of neighbored molecules in crystals of **7**/**10** are parallel. In crystals of **7** the fused benzene portions share the most overlap (plane···plane distance 3.49 Å, centroid···centroid distance 3.67 Å; 18.2°). Quite similar values were found for the π–π interactions between the fused benzene rings in crystals of **10** (plane···plane distance 3.49 Å; centroid···centroid distance 3.62 Å; displacement angle 15.1°).

Furthermore weak intermolecular N–H···Br hydrogen bonds between neighboring molecules were found in crystals of **7** (Fig. 8b). Compared with the aforementioned intramolecular hydrogen bonds (Table 4) the N···Br distance of 3.38(1) Å indicates that the intermolecular hydrogen bonds are weaker than the intramolecular ones.

### 2.3.2. Molecular structure of the dinuclear complex *11*

The crystal structure of the dinuclear compound **11**, $[PPh_4][(PtBrMe_2)_2(\mu\text{-}Br)(\mu\text{-}pz)_2]$, consists of discrete ions. There is no evidence of unusual interionic interactions. The arrangement of the anion is illustrated in Fig. 9 and selected bond lengths and angles are given in Table 5.

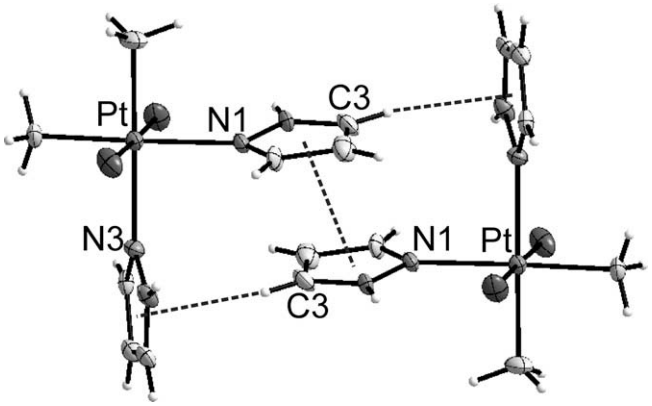


**Fig. 7.** Illustration of face-to-edge and π–π interaction between molecules in the solid-state structure of **5**. Displacement ellipsoids at 30% probability.

Two methyl ligands, a terminal and a bridging bromo ligand and two bridging pyrazolato ligands surround each platinum in an approximate octahedral arrangement. The interplanar angles of the least-squares planes of the pyrazolato rings to the equatorial $[PtC_2N_2]$ planes are between 52.1(5)° and 56.6(5)°. Although the octahedral arrangement around the Pt2 atom is more distorted (Br3–Pt2–Br2 177.6(1)°) than the arrangement around Pt1 (C–Pt1–N 178.9(4)°), no unusual deviation from the expected angles is observed. The distance between the platinum(IV) centers is 3.593(1) Å, eliminating the possibility of a direct interaction between them.

To date only three crystal structures with platinum(IV) bridged to a second metal center *via* pyrazolato ligands have been published [1d,8]. The Pt–C bond lengths in **11** are comparable with those found in similar structures [1d,8]. In addition, the Pt–C bond lengths of **11** are slightly longer than the same bonds in mononuclear **5** with pyrazole ligands. This may be correlated with the smaller $^2J_{Pt,H}$ coupling constant found for Pt–C$H_3$ of **11** (66.6 Hz) relative to that found for **5** (72.4 Hz), indicating the stronger *trans*

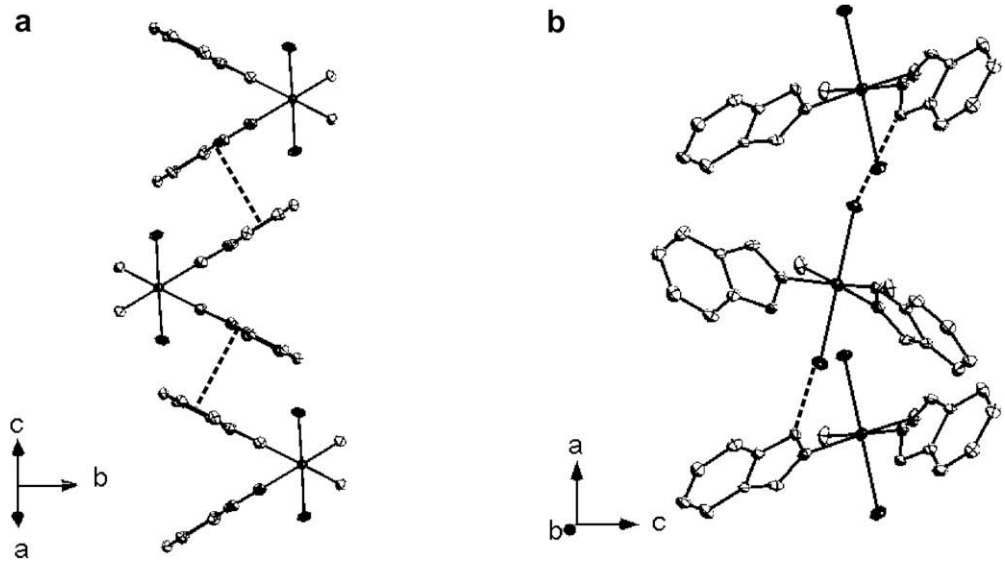


**Fig. 8.** π–π interactions between parallel indazole ligands (a) and hydrogen bonding (b) within the solid-state structure of **7**. Displacement ellipsoids at 30% probability, hydrogen atoms omitted for clarity.

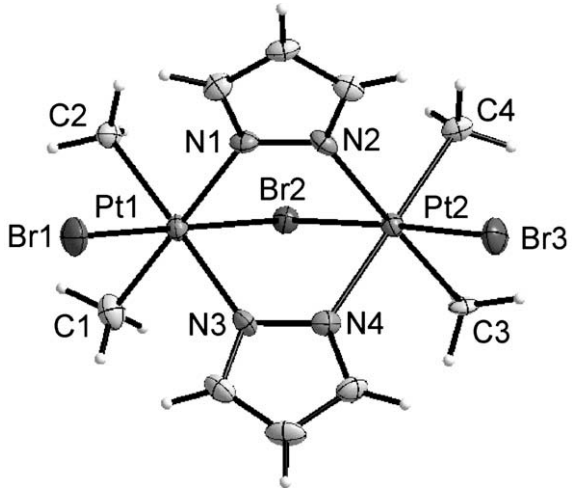


**Fig. 9.** Molecular structure of $[(PtBrMe_2)_2(\mu\text{-}Br)(\mu\text{-}pz)_2]^-$ anion in the solid-state structure of **11**. Displacement ellipsoids at 30% probability.

**Table 5**
Selected angles and bond lengths for **11**

| Selected bond lengths (Å) | | Selected bond angles (°) | |
|---|---|---|---|
| Pt1–C | 2.12(1)/2.13(1) | C–Pt1–N | 178.9(4)/179.9(4) |
| Pt2–C | 2.15(1)/2.13(1) | C–Pt2–N | 179.4(4)/178.3(4) |
| Pt1–N | 2.167(8)/2.144(9) | N–Pt1–N | 89.1(3) |
| Pt2–N | 2.162(9)/2.162(9) | N–Pt2–N | 88.8(3) |
| Pt1–Br1/Br2 | 2.413(1)/2.502(1) | Br–Pt1–Br | 179.2(1) |
| Pt2–Br3/Br2 | 2.405(1)/2.493(1) | Br–Pt2–Br | 177.6(1) |

influence of the μ-pyrazolato relative to the neutral pyrazole ligand, as is expected. The Pt–N as well as the terminal and bridging Pt–Br bond lengths in **11** show no significant differences from reported bond lengths of these types [7,8,20].

## 3. Summary

A series of platinum(IV) mononuclear complexes with the $PtBr_2Me_2$ moiety and aromatic nitrogen donor ligands were prepared and characterized. The crystal structures of these complexes illustrated many weak inter- and intramolecular interactions, which are favourable with such heteroaromatic systems [24]. The preparation of dinuclear platinum(IV) complexes using mononuclear starting complexes was demonstrated by the syntheses of two homodinuclear platinum(IV) compounds. The neutral μ-bipyrimidine complex **12**, $[(PtBr_2Me_2)_2(\mu\text{-bpym})]$, was characterized in solution, although it was found to decompose in solvents with high donor capability. The μ-pyrazolato complex **11**, $[PPh_4][(PtBrMe_2)_2(\mu\text{-}Br)(\mu\text{-}pz)_2]$, was characterized both in solution and by X-ray diffraction, the first solid-state structure of a dimethylplatinum(IV) complex of this type.

## 4. Experimental

### 4.1. General comments

All reactions were performed under an argon atmosphere using the standard Schlenk techniques. Reactions were carried out in dried solvents ($CHCl_3$ over $CaH_2$, MeOH over $Mg/NaBH_4$/Fepc ($H_2pc$ = phthalocyanine) distilled prior to use. $^1H$ and $^{13}C$ NMR spectra were recorded on Varian Gemini 2000 (200 and 400 MHz) and Varian Unity 500 (500 MHz) spectrometers. $^1H$ and $^{13}C$ NMR chemical shifts are relative to solvent signals: chloroform-$d_1$ $\delta_H$ 7.24, $\delta_C$ 77.0; methanol-$d_4$ $\delta_H$ 3.30, $\delta_C$ 49.0; DMF-$d_7$ $\delta_H$ 2.74, $\delta_C$ 30.1 and acetone-$d_6$ $\delta_H$ 2.04, $\delta_C$ 29.8. Assignment of NMR signals was partially revealed by COSY, HMBC and NOE experiments. $^{195}Pt$ NMR data are referenced relative to $H_2[PtCl_6]$ in $D_2O$ ($\delta_{Pt}$ 0). IR spectra were recorded on a Galaxy Mattson 5000 FT-IR spectrometer using KBr pellets. Microanalyses were performed at the microanalytical laboratory of Martin-Luther-Universität Halle-Wittenberg using CHNS-932 (LECO) and Vario EL (Elementaranalysensysteme) elemental analyzers. TG and DTA were preformed on a STA 449C (Netzsch). Argon was used as the protective and purge gas (30 ml/min). Samples were heated to 1000 °C at a heating rate of 10 K/min in an $Al_2O_3$ crucible. EI–MS was determined by slow heating of samples to a maximum of 350 °C and an ionisation energy of 70 eV on an AMD 402 (AMD Intectra GmbH). ESI-MS for **11** and **12** was recorded on a Finnigan Mat spectrometer LCQ using the following conditions: carrier gas: $N_2$, flow rate: 8 μl/min, spray voltage: 4.1 kV, temperature of the

capillary: 150 °C, voltage of the capillary: 34 V. 2,2′-Bipyridine and its derivatives, bipyrimidine, pyrazole, 4-methyl-pyrazole, imidazole, indazole, benzimidazole, quinazoline and tetraphenylphosphonium bromide were used as purchased (Aldrich/Acros). 2,2′-Bipyrazine and $[(PtBr_2Me_2)_n]$ were prepared as described in the literature [25,3].

#### 4.1.1. General procedure for the synthesis of **1–10**

$[(PtBr_2Me_2)_n]$ (52 mg, 0.14 mmol) and the appropriate ligand (0.14 mmol) were added to a Schlenk flask. The reagents were allowed to stir under Ar at ambient temperature in $CHCl_3$ (10 ml) for 24 h or until the reaction mixture became transparent. The yellow colored solution was then evaporated to dryness. The residue was dissolved in a minimum of $CHCl_3$ (ca. 2 ml) and the product was precipitated on addition of *n*-pentane (ca. 8 ml). 2 mol equivalents of the ligand were used for **5–10**. Deviations from this procedure are given in each case.

#### 4.1.2. $[PtBr_2Me_2(4,4'\text{-di-Me-}2,2'\text{-bpy})]$ (**1**)

Yellow powder. Yield: 69 mg (73%). $T_{dec}$ 251–254 °C; $\Delta m$ 16.7% (calc. for MeBr). Found: 15.6%. *Anal.* Calc. for $C_{14}H_{18}Br_2N_2Pt$ (569.19): C, 29.54; H, 3.19; N, 4.92. Found: C, 29.30; H, 3.25; N, 4.84%. IR ($cm^{-1}$): $\nu$ 3448 (s), 2964 (w), 2904 (m), 1616 (s), 1487 (w), 1444 (m), 1410 (m), 1248 (w), 1026 (s), 835 (s), 553 (w), 521 (w). $^1$H NMR (400 MHz, $CDCl_3$): $\delta$ 2.11 (s+d, $^2J_{Pt,H}$ = 70.8 Hz, 6H, PtC$H_3$), 2.59 (s, 6H, C$^4$C$H_3$), 7.47 (d, $^3J_{H,H}$ = 5.6 Hz, 2H, C$^3H$), 8.03 (s, 2H, C$^5H$), 8.75 (d+dd, $^3J_{H,H}$ = 5.6 Hz, $^3J_{Pt,H}$ = 11.7 Hz, 2H, C$^6H$). $^{13}$C NMR (125 MHz, $CDCl_3$): $\delta$ −6.1 (s+d, $^1J_{Pt,C}$ = 518.6 Hz, PtCH$_3$), 21.7 (s, C$^4$CH$_3$), 124.2 (s+d, $^3J_{Pt,C}$ = 7.4 Hz, C$^3$H), 127.6 (s+d, $^3J_{Pt,C}$ = 11.8 Hz, C$^5$H), 146.7 (s+d, $^2J_{Pt,C}$ = 13.3 Hz, C$^6$H), 151.2 (s, C$^4$CH$_3$), 154.5 (s, C$^2$). $^{195}$Pt NMR (107 MHz, $CDCl_3$): $\delta$ −2550 (s). EI-MS: calc. *m/z* for ($[C_{14}H_{18}Br_2N_2Pt]^{+\cdot}$) 570; found 570; *m/z* (Intensity calc./found) for cationic radical $[C_{14}H_{18}Br_2N_2Pt]^{+\cdot}$, %) 566 (34/36), 567 (39/34), 568 (96/99), 569 (81/69), 570 (100/100), 571 (47/43), 572 (44/42), 572 (6/7).

#### 4.1.3. $[PtBr_2Me_2(4,4'\text{-di-t-Bu-}2,2'\text{-bpy})]$ (**2**)

Yellow microcrystalline solid. Yield: 70 mg (87%). $T_{dec}$ 245–250 °C; $\Delta m$ 13.6% (calc. for MeBr). Found: 14.5%. *Anal.* Calc. for $C_{20}H_{30}Br_2N_2Pt$ (653.35): C, 36.77; H, 4.63; N, 4.29. Found: C, 36.45; H, 4.59; N, 4.13%. IR ($cm^{-1}$): $\nu$ 3438 (s), 2966 (s), 2906 (s), 2361 (s), 2335 (s), 1617 (s), 1551 (w), 1460 (m), 1410 (s), 1261 (m), 1092 (s), 1025 (s), 883 (w), 801 (m), 661 (w). $^1$H NMR (400 MHz, $CDCl_3$): $\delta$ 1.44 (s, 18H, C(C$H_3$)$_3$), 2.12 (s+d, $^2J_{Pt,H}$ = 70.6 Hz, 6H, PtC$H_3$), 7.50–7.63 (m, 2H, C$^5H$), 8.15 (s, 2H, C$^3H$), 8.74 (m, 2H, C$^6H$). $^{13}$C NMR (125 MHz, $CDCl_3$): $\delta$ −6.2 (s+d, $^1J_{Pt,C}$ = 515.7 Hz, PtCH$_3$), 30.5 (s, C(CH$_3$)$_3$), 35.5 (s, C(CH$_3$)$_3$), 120.2 (s+d, $^3J_{Pt,C}$ = 8.8 Hz, C$^3$H), 124.3 (s+d, $^3J_{Pt,C}$ = 13.3 Hz, C$^5$H), 146.9 (s+d, $^2J_{Pt,C}$ = 13.3 Hz, C$^6$H), 154.7 (s, C$^4$C(CH$_3$)$_3$), 163.9 (s, C$^2$). $^{195}$Pt NMR (107 MHz, $CDCl_3$): $\delta$ −2556 (s). EI-MS: calc. *m/z* for ($[C_{20}H_{30}Br_2N_2Pt]^{+\cdot}$) 654; found 654; *m/z* (Intensity calc./found) for cationic radical $[C_{20}H_{30}Br_2N_2Pt]^{+\cdot}$, %) 650 (32/33), 651 (39/36), 652 (93/95), 653 (83/77), 654 (100/100), 655 (51/51), 656 (45/41), 657 (9/10), 658 (7/8).

#### 4.1.4. $[PtBr_2Me_2(2,2'\text{-bpz})]$ (**3**)

As in Section 4.1.1. except $CHCl_3$ (50 ml). Filtered the reaction mixture before precipitating an orange powder from $CHCl_3$/pentane. Yield: 47 mg (94%). $T_{dec}$ 198–201 °C; $\Delta m$ 17.5% (calc. for MeBr). Found: 15.5%. *Anal.* Calc. for $C_{10}H_{12}Br_2N_4Pt$ (543.12): C, 22.11; H, 2.23; N, 10.32. Found: C, 21.66; H, 2.30; N, 9.83%. IR ($cm^{-1}$): $\nu$ 3418 (m), 3050 (w), 2908 (w), 1404 (s), 1308 (w), 1157 (s), 1047 (s), 843 (m), 472 (s). $^1$H NMR (500 MHz, $CDCl_3$): $\delta$ 2.21 (s+d, $^2J_{Pt,H}$ = 72.9 Hz, 6H, C$H_3$), 8.89–8.90 (dd+ddd(br), $^3J_{H,H}$ = 2.8 Hz, $^5J_{H,H}$ = 1.4 Hz, 2H, C$^6H$), 9.06 (d, $^3J_{H,H}$ = 2.8 Hz, 2H, C$^5H$), 9.70 (d, $^3J_{H,H}$ = 1.3 Hz, 2H, C$^3H$). $^{13}$C NMR (100 MHz, $CDCl_3$): $\delta$ −4.6 (s, C$H_3$), 141.2 (s, C$^6$H), 145.0 (s, C$^3$H), 147.4 (s, C$^2$), 148.7 (C$^5$H). $^{195}$Pt NMR (107 MHz, $CDCl_3$): $\delta$ −2668 (s). EI-MS *m/z* for ($[C_{10}H_{12}Br_2N_4Pt]^{+\cdot}$) 543; found 543; *m/z* (Intensity calc./found) for cationic radical $[C_{10}H_{12}Br_2N_4Pt]^{+\cdot}$, %) 540 (35/35), 541 (39/40), 542 (97/97), 543 (80/79), 544 (100/100), 545 (47/47), 546 (45/45).

#### 4.1.5. $[PtBr_2Me_2(bpym)]$ (**4**)

Yellow powder. Yield: 67 mg (61%). $T_{dec}$ 212–216 °C; $\Delta m$ 17.5% (calc. for MeBr). Found: 19.0%. *Anal.* Calc. for $C_{10}H_{12}Br_2N_4Pt$ (543.12): C, 22.11; H, 2.23; N, 10.32. Found: C, 22.00; H, 2.44; N, 9.63%. IR ($cm^{-1}$): $\nu$ 3418 (m), 3048 (w), 2905 (w), 1573 (s), 1555 (s), 1406 (s), 1228 (w), 1100 (w), 1013 (w), 756 (m), 686 (m), 669 (m). $^1$H NMR (400 MHz, $(D_3C)_2NCDO$): $\delta$ 2.20 (s+d, $^2J_{Pt,H}$ = 72.8 Hz, 6H, C$H_3$), 8.25 (t, $^3J_{H,H}$ = 5.1 Hz, 2H, C$^5$H), 9.47–9.49 (m, 2H, C$^6$H), 9.51–9.53 (m, 2H, C$^4$H). $^{13}$C NMR (125 MHz, $(D_3C)_2NCDO$): $\delta$ −6.6 (s+d, $^1J_{Pt,C}$ = 529.9 Hz, C$H_3$), 125.8 (s+d, $^3J_{Pt,C}$ = 10.4 Hz C$^5$H), 155.6 (s+d, $^2J_{Pt,C}$ = 10.4 Hz C$^6$H), 161.3 (s, C$^2$), 161.9 (s, C$^4$H). $^{195}$Pt NMR (107 MHz, $(D_3C)_2NCDO$): $\delta$ −2613 (s). EI-MS calc. *m/z* for ($[C_{10}H_{12}Br_2N_4Pt]^{+\cdot}$) 544; found 544; *m/z* (Intensity calc./found) for cationic radical $[C_{10}H_{12}Br_2N_4Pt]^{+\cdot}$, %) 540 (36/41), 541 (40/43), 542 (98/92), 543 (80/79), 544 (100/100), 545 (45/46), 546 (44/47), 547 (5/12).

#### 4.1.6. $[PtBr_2Me_2(H\text{-pz})_2]$ (**5**)

Yellow microcrystalline solid. Yield: 110 mg (98%). $T_{dec}$ 132–136 °C; $\Delta m$ 18.2% (calc. for MeBr). Found: 20.5%. *Anal.* Calc. for $C_8H_{14}Br_2N_4Pt$ (521.11): C, 18.44; H, 2.71; N, 10.75. Found: C, 19.10; H, 2.88; N, 10.87%. IR ($cm^{-1}$): $\nu$ 3345 (s), 2907 (s), 1466 (w), 1390 (m), 1357 (s), 1119 (m), 1043 (s), 758 (s), 679 (m), 581 (m). $^1$H NMR (400 MHz, $CDCl_3$): $\delta$ 1.84 (s+d, $^2J_{Pt,H}$ = 72.4 Hz, 6H, C$H_3$), 6.37 (m, 2H, C$^4H$), 7.58 (s, 2H, C$^5H$), 8.18 (m, 2H, C$^3H$), 11.20 (s(br), 2H, N$^1H$); $^{13}$C NMR (100 MHz, $CDCl_3$): $\delta$ −10.4 (s+d, $^1J_{Pt,C}$ = 504.9, C$H_3$), 106.9 (s+d, $^3J_{Pt,C}$ = 9.7 Hz, C$^4H$), 129.2 (s+d, $^3J_{Pt,C}$ = 6.5 Hz, C$^5$H), 139.2 (s+d, $^2J_{Pt,C}$ = 11.8 Hz, C$^3H$); $^{195}$Pt NMR (107 MHz, $CDCl_3$): $\delta$ 2431 (s). EI-MS: calc. *m/z* for ($[C_8H_{14}Br_2N_4Pt]^{+\cdot}$) 521; found 521; *m/z* (Intensity calc./found) for cationic radical ($[C_8H_{14}Br_2N_4Pt]^{+\cdot}$, %) 518 (36/29), 519 (39/46), 520 (98/91), 521 (79/61), 522 (100/100), 523 (43/36), 524 (43/42).

#### 4.1.7. $[PtBr_2Me_2(4\text{-Me-}H\text{-pz})_2]$ (**6**)

Bright yellow microcrystalline solid from $CHCl_3$/hexane at −18 °C. Yield: 44 mg (74%). $T_{dec}$ 127–132 °C; $\Delta m$ 17.3% (calc. for MeBr). Found: 18.8%. *Anal.* Calc. for $C_{10}H_{18}Br_2N_4Pt$ (549.16): C, 21.87; H, 3.30; N, 10.20. Found: C, 22.06; H, 3.45; N, 10.23%. IR ($cm^{-1}$): $\nu$ 2912 (w), 1475 (w), 1390 (w), 1227 (s), 1168 (s), 1059 (s), 999 (s), 966 (m), 821 (w), 657 (s), 543 (m). $^1$H NMR (400 MHz, $CDCl_3$): $\delta$ 1.86 (s+d, $^2J_{Pt,H}$ = 72.2 Hz, 6H, PtC$H_3$), 2.07 (s, 6H, C$^4$C$H_3$), 7.33 (s, 2H, C$^5H$), 7.95 (s, 2H, C$^3H$), 11.12 (s(br), 2H, N$^1H$). $^{13}$C NMR (125 MHz, $CDCl_3$): $\delta$ −10.8 (s+d, $^1J_{Pt,C}$ = 501.4 Hz, PtCH$_3$), 8.8 (s, C$^4$CH$_3$), 117.3 (s, C$^4$CH$_3$), 128.2 (s, C$^5$H), 139.2 (s, C$^3$H). $^{195}$Pt NMR (107 MHz, $CDCl_3$): $\delta$ −2417 (s). EI-MS: calc. *m/z* for ($[C_8H_{18}Br_2N_4Pt]^{+\cdot}$) 549; found 549; *m/z* (Intensity calc./found) for cationic radical $[C_{10}H_{18}Br_2N_4Pt]$–$H_2)^{+\cdot}$, %) 544 (35/41), 545 (39/47), 546 (97/91), 547 (80/79), 548 (100/100), 549 (45/52), 550 (44/43), 551 (5/10).

#### 4.1.8. $[PtBr_2Me_2(H\text{-idz})_2]$ (**7**)

Product isolated directly after removal of solvent, yellow microcrystalline solid. Yield: 112 mg (100%). $T_{dec}$ 176–180 °C; $\Delta m$ 15.3% (calc. for MeBr). Found: 17.2%. *Anal.* Calc. for $C_{16}H_{18}Br_2N_4Pt$ (621.23): C, 30.93; H, 2.92; N, 9.02. Found: C, 31.45; H, 3.12; N, 9.06%. IR ($cm^{-1}$): $\nu$ 3346 (s), 2910 (s), 1627 (m), 1511 (m), 1355 (s), 1243 (m), 1088 (s), 960 (m), 857 (w), 750 (s), 650 (s), 428 (m), 310 (m). $^1$H NMR (400 MHz, $CDCl_3$): $\delta$ 2.04 (s+d,

$^2J_{Pt,H}$ = 72.6 Hz, 6H, C$H_3$), 7.18 (m, 2H, C$^6H$), 7.46 (m, 2H, C$^{7/8}H$), 7.74 (d, $^3J_{H,H}$ = 8.3 Hz, 2H, C$^5H$), 8.77 (s(br), 2H, C$^3H$), 11.34 (s(br), 2H, N$^1H$). $^{13}$C NMR (125 MHz, $CDCl_3$): $\delta$ −9.6 (s+d, $^1J_{Pt,C}$ = 502.9 Hz, C$H_3$), 110.2 (s, C$^6$H), 121.5 (s, C$^4$H), 122.3 (s, C$^5$H), 123.1 (s, C$^{3a}$), 135.1 (s+d, $^3J_{Pt,C}$ = 10.7 Hz, C$^3$H), 139.9 (s, C$^{7a}$). $^{195}$Pt NMR (107 MHz, $CDCl_3$): $\delta$ −2458 (s). EI-MS: calc. *m/z* for ($[C_{16}H_{18}Br_2N_4Pt]^{+\cdot}$) 622; found 622; *m/z* (Intensity calc./found) for cationic radical ($[C_{16}H_{18}Br_2N_4Pt]-H_2)^{+\cdot}$, %) 616 (33/36), 617 (39/40), 618 (95/92), 619 (82/78), 620 (100/100), 621 (49/49), 622 (44/41), 623 (7/10), 624 (8/7).

#### 4.1.9. [$PtBr_2Me_2$(H-im)$_2$] (**8**)

Yellow solid residue. Yield (crude): 18 mg (100%). $^1$H NMR (400 MHz, $CD_3OD$) 1.79 (s+d, $^2J_{Pt,H}$ = 70.6 Hz, 6H, C$H_3$), 7.04 (s, 2H, C$H$), 7.41 (s(br), 2H, C$H$), 8.06 (s(br), CH, C$H$). $^{13}$C NMR (125 MHz, $CD_3OD$) −10.8 (s+d, $^1J_{Pt,C}$ = 506.7 Hz, C$H_3$), 117.3 (s+d, $J_{Pt,C}$ = 11.7 Hz), 128.5 (s+d, $J_{Pt,C}$ = 7.9 Hz), 138.2 (s+d, $J_{Pt,C}$ = 17.6 Hz). $^{195}$Pt NMR (107 MHz, $CD_3OD$) −2340 (s).

#### 4.1.10. [$PtBr_2Me_2$(H-bim)$_2$] (**9**)

Bright yellow microcrystalline solid from acetone/pentane at −18 °C. Yield: 94 mg (85%). $T_{dec}$ 157–159 °C; $\Delta m$ 15.3% (calc. for MeBr). Found: 12.8%. *Anal.* Calc. for $C_{16}H_{18}Br_2N_4Pt$ (621.23): C, 30.93; H, 2.92; N, 9.02. Found: C, 30.85; H, 3.26; N, 8.68%. IR ($cm^{-1}$): *v* 3224 (s), 2979 (w), 2904 (m), 1622 (w), 1504 (s), 1417 (s), 1306 (m), 1254 (s), 968 (w), 740 (s), 442 (m). $^1$H NMR (400 MHz, $(D_3C)_2CO$): $\delta$ 2.16 (s+d, $^2J_{Pt,H}$ = 71.4 Hz, 6H, C$H_3$), 7.00–7.04 (m, 2H, C$^5H$), 7.20–7.24 (m, 2H, C$^6H$), 7.60–7.63 (m, 2H, C$^7H$), 7.80–7.82 (m, 2H, C$^4H$), 8.56 (s+d, $^3J_{Pt,H}$ = 7.9 Hz, 2H, C$^2H$) 12.15 (s(br), 2H, N$^1H$). $^{13}$C NMR (100 MHz, $(D_3C)_2CO$): $\delta$ −8.1 (s+d, $^1J_{Pt,C}$ = 517.8 Hz, C$H_3$), 113.8 (s, C$^7$H), 121.3 (s, C$^4$H), 123.0 (s, C$^5$H), 124.4 (s, C$^6$H), 133.9 (s, C$^{7a}$), 140.7 (s, C$^{3a}$), 146.0 (s+d, $^2J_{Pt,C}$ = 14.9 Hz, C$^2$H). $^{195}$Pt NMR (107 MHz, $(D_3C)_2CO$): $\delta$ −2308 (s).

#### 4.1.11. [$PtBr_2Me_2$(quaz)$_2$] (**10**)

Yellow powder. Yield: 19 mg (45%). $T_{dec}$ 160–163 °C; $\Delta m$ 24.7% (calc. for $Br_2$). Found: 22.4%. *Anal.* Calc. for $C_{18}H_{18}Br_2N_4Pt$ (645.25): C, 33.51; H, 2.81; N, 8.68. Found: C, 32.74; H, 3.01; N, 8.63%. IR ($cm^{-1}$): *v* 2975 (w), 2908 (s), 2809 (w), 1621 (s), 1585 (s), 1488 (m), 1378 (s), 1309 (w), 1211 (m), 1155 (s), 1062 (w), 962 (m), 929 (m), 873 (w), 788 (s), 752 (s), 634 (s), 543 (w), 487 (w). $^1$H NMR (400 MHz, $CDCl_3$): $\delta$ 2.21 (s+d, $^2J_{Pt,H}$ = 71.8 Hz, 6H, C$H_3$), 7.77 (m, 2H, C$^7H$), 8.02–8.08 (m, 6H, C$^{5/6/8}H$), 9.55 (s(br), 2H, C$^2H$), 9.96 (s+d, $^3J_{Pt,H}$ = 14.5 Hz, 2H, C$^4H$). $^{13}$C NMR (125 MHz, $CDCl_3$): $\delta$ −7.8 (s, C$H_3$), 124.7 (s, C$^{8a}$), 128.4# (s, C$H$), 128.4# (s, C$H$), 129.3 (s, C$^7$H), 136.7 (s, C$^5$H), 149.8 (s, C$^{4a}$), 154.5# (s(br), C$H$), 161.4# (s(br), C$H$). $^{195}$Pt NMR (107 MHz, $CDCl_3$): $\delta$ −2413 (s). # – not distinguishable by NOE, HMBC or COSY experiments.

#### 4.1.12. Synthesis of [$PPh_4$][($PtBrMe_2$)$_2$($\mu$-Br)($\mu$-pz)$_2$] (**11**)

To a transparent solution of **5** (14 mg, 0.02 mmol) in MeOH (5 ml) 2 equiv. of a solution of KOH in MeOH (1.05 M) were added. The mixture was stirred for at least 72 h. To this mixture $[(PtBr_2Me_2)_n]$ (9 mg, 0.02 mmol) was added and the reaction mixture was allowed to stir a further 48 h. To the transparent reaction mixture at 0 °C, a solution of $[PPh_4]Br$ (9 mg, 0.02 mmol) in $CHCl_3$ (1 ml) was added. A yellow precipitate formed, was filtered, washed with a small portion of ice cold MeOH (3 ml) and dried under vacuum to yield a yellow microcrystalline solid. Yield: 15 mg (56%). $T_{dec}$ 198–200 °C; $\Delta m$ 8.2% (calc. for MeBr). Found: 8.4%. *Anal.* Calc. for $C_{34}H_{38}Br_3N_4PPt_2$ (1163.53): C, 35.10; H, 3.29; N, 4.82. Found: C, 34.16; H, 3.45; N, 4.54%. IR ($cm^{-1}$): *v* 2901 (m), 1437 (m), 1110 (s), 1051 (s), 724 (m), 689 (m), 526 (s). $^1$H NMR (400 MHz, $CDCl_3$): $\delta$ 1.72 (s+d, $^2J_{Pt,H}$ = 66.6 Hz, 12H, C$H_3$), 5.83 (s(br), 2H, C$^4H$), 7.42–7.54 (m, 16H, Ph–*H*), 7.58 (d(br), $^3J_{H,H}$ = 1.9 Hz, 4H, C$^{3/5}H$), 7.75–7.78 (m, 4H, Ph–*H*). $^{13}$C NMR (125 MHz, $CDCl_3$): $\delta$ −12.6 (s, C$H_3$), 103.6 (s, C$^4$H), 116.9 (d, $J_{P,C}$ = 89.7 Hz, Ph–*C*), 130.5 (d, $J_{P,C}$ = 12.9 Hz, Ph–*C*), 134.2 (d, $J_{P,C}$ = 10.2 Hz, Ph–*C*), 135.8 (d, $J_{P,C}$ = 2.7 Hz, Ph–*C*), 136.8 (s(br), C$^{3/5}$H). $^{195}$Pt NMR (107 MHz, $CDCl_3$): $\delta$ −2287 (s). Negative mode ESI-MS: ($CH_2Cl_2$) calc. *m/z* for $[C_{10}H_{18}Br_3N_4Pt_2]^-$ 824. Found: $[C_{10}H_{18}Br_3N_4Pt_2]^-$ 824; *m/z* (Intensity calc./found) for ($[C_{10}H_{18}Br_3N_4Pt_2]^-$, %) 821 (45/47), 822 (64/66), 823 (97/88), 824 (94/83), 825 (100/100), 826 (70/59), 827 (56/44), 828 (27/17). Positive mode ESI-MS: ($CH_2Cl_2$) calc. *m/z* for $[C_{24}H_{20}P]^+$ 339. Found: $[C_{24}H_{20}P]^+$ 339.

#### 4.1.13. Synthesis of [($PtBr_2Me_2$)$_2$($\mu$-bpym)] (**12**)

$[(PtBr_2Me_2)_n]$ (39 mg, 0.10 mmol) and bipyrimidine (8 mg, 0.05 mmol) were stirred in $CHCl_3$ (3 ml) for 30 h. Alternatively, $[(PtBr_2Me_2)_n]$ (19 mg, 0.05 mmol) and **4** (28 mg, 0.05 mmol) were stirred in $CHCl_3$ (3 ml) for 24 h. In either case, the resulting powder was then filtered and washed with portions of $CHCl_3$ (2 × 5 ml) and MeOH (1 × 10 ml). The dark yellow powder was dried under vacuum. Yield: 47 mg (100%). $T_{dec}$ 255–258 °C; $\Delta m$ 17.2% (calc. for $Br_2$). Found: 18.0%. *Anal.* Calc. for $C_{34}H_{38}Br_3N_4PPt_2$ (928.07): C, 15.53; H, 1.95; N, 6.04. Found: C, 15.29; H, 2.03; N, 5.50%. IR ($cm^{-1}$): *v* 3443 (m), 3072 (w), 2904 (m), 1576 (s), 1416 (s), 1259 (w), 1140 (w), 1034 (m), 813 (m), 742 (m), 684 (w). $^1$H NMR (400 MHz, $(D_3C)_2NCDO$): $\delta$ 2.25 (s+d, $^2J_{Pt,H}$ = 74.7 Hz, 12H, C$H_3$), 8.73 (t, $^3J_{H,H}$ = 5.4 Hz, 2H, C$^5H$), 9.90 (d, $^3J_{H,H}$ = 5.4 Hz, 4H, C$^{4/6}H$); signals from **4**: $\delta$ 2.11 (s+d, $^2J_{Pt,H}$ = 72.6 Hz, 6H, C$H_3$), 8.73 (t, $^3J_{H,H}$ = 5.2 Hz, 2H, C$^5H$), 9.47–9.50 (m, 4H, C$^{4/5}H$); [$PtBr_2Me_2$(DMF-$d_7$)$_2$] 2.03 (s+d, $^2J_{Pt,H}$ = 79.5 Hz, C$H_3$). $^{195}$Pt NMR (107 MHz, $(D_3C)_2NCDO$): $\delta$ −1896 (s, [$PtBr_2Me_2$(DMF-$d_7$)$_2$]) −2613 (s, **4**), −2618 (s, **12**). Negative mode ESI-MS: (MeOH) calc. *m/z* for $[C_{12}H_{18}Br_4N_4Pt_2]$ 928.08. Found: $[C_{12}H_{18}Br_4N_4Pt_2{+}OCH_3]^-$ 954.8 (954.76); *m/z* (Intensity calc./found) for $[C_{12}H_{18}Br_4N_4Pt_2{+}OCH_3]^-$, %) 957 (72/56), 958 (81/56), 959 (100/100), 960 (85/74), 961 (80/74), 962 (50/45). Positive mode ESI-MS: (MeOH) Calc. *m/z* for $[C_{12}H_{18}Br_4N_4Pt_2]$ 928.07. Found: $[C_{12}H_{18}Br_4N_4Pt_2{+}Na]^+$ 950.5 (951.06); *m/z* (Intensity calc./found) for $[C_{12}H_{18}Br_4N_4Pt_2{+}Na]^+$, %) 947 (28/27), 948 (42/47), 949 (72/73), 950 (81/85), 951 (100/100), 952 (84/71), 953 (79/39).

### 4.2. X-ray crystallography

Pink crystals of **2** and yellow crystals of **5** and **7** suitable for X-ray crystallographic measurements were obtained by slow evaporation of a chloroform solution of the respective complex. Dark yellow crystals of **6** were obtained by slow evaporation of a dichloromethane solution of **6**. Complex **10** crystallized as small cube-like yellow crystals by slow evaporation of a chloroform/pentane solution. Yellow cube-like crystals of **11** were obtained by slow evaporation of a methanol/chloroform solution from the mother-liquor. Tables 6 and 7 show crystallographic data and collection parameters.

Intensity data were collected on a STOE-STADI IV at 293(2) K (**2**), STOE-IPDS (**5**, **9**, **7**, **11**) at 220(2) K or on a CCD Oxford Xcalibur S diffractometer (**6**) at 130(2) K all with Mo K$\alpha$ radiation ($\lambda$ = 0.7103 Å, graphite monochromator). Absorption corrections for **5**, **9**, **7** and **11** were made using the IPDS software package and absorption correction of **2** was made with X-RED32 [26a,b]. A semi-empirical correction was made for **6** with SCALE3 ABSPACK [26c]. All structures were solved by direct methods with SHELX-97 [27a] and refined using full-matrix least-square routines against $F^2$ with SHELXL-97 [27b]. Non-hydrogen atoms were refined with anisotropic displacement parameters. Hydrogen atoms were included in the models by calculating the positions (riding model) and refined with calculated isotropic displacement parameters. Illustrations were generated using DIAMOND 3.0 software [28].

**Table 6**
Crystallographic and data collection parameters for complexes **2**, **5** and **6**

| Complex | **2** | **5** | **6** |
|---|---|---|---|
| Empirical formula | $C_{20}H_{30}Br_2N_2Pt$ | $C_8H_{14}Br_2N_4Pt$ | $C_{10}H_{18}Br_2N_4Pt$ |
| Formula weight | 653.37 | 521.14 | 549.19 |
| Crystal system | orthorhombic | triclinic | orthorhombic |
| Space group | *Cmca* | *P*$\bar{1}$ | *Pcca* |
| *Z* | 8 | 2 | 4 |
| *a* (Å) | 13.755(2) | 7.127(2) | 12.757(1) |
| *b* (Å) | 20.249(3) | 8.138(2) | 8.376(1) |
| *c* (Å) | 16.693(1) | 12.007(3) | 14.085(1) |
| $\alpha$ (°) | 90 | 85.07(3) | 90 |
| $\beta$ (°) | 90 | 84.01(3) | 90 |
| $\gamma$ (°) | 90 | 73.34(3) | 90 |
| *V* (Å$^3$) | 4649.3(9) | 662.4(3) | 1505.0(1) |
| $\rho$ (g cm$^{-3}$) | 1.867 | 2.613 | 2.424 |
| $\mu$ (Mo K$\alpha$) (mm$^{-1}$) | 9.48 | 16.60 | 14.62 |
| *F*(000) | 2496 | 476 | 1016 |
| Scan range (°) | 2.01 < $\theta$ < 25.97 | 2.62 < $\theta$ < 25.89 | 2.89 < $\theta$ < 28.27 |
| Reciprocal lattice segments *h*, *k*, *l* | −8 → 16 | −8 → 8 | −16 → 17 |
| | 0 → 24 | −9 → 9 | −10 → 11 |
| | 0 → 20 | −14 → 14 | −18 → 18 |
| Reflections collected | 4247 | 3947 | 14343 |
| Reflections independent | 2386 | 2355 | 1874 |
| Observed reflections | 1791 | 1891 | 1207 |
| Data/restraints/parameters | 2386/0/120 | 2355/0/139 | 1874/0/80 |
| Goodness-of-fit on $F^2$ | 1.108 | 1.037 | 0.957 |
| $R_1$, $wR_2$ [$I > 2\sigma(I)$] | 0.0436, 0.0867 | 0.0584, 0.1539 | 0.0215, 0.0404 |
| $R_1$, $wR_2$ (all data) | 0.0728, 0.1006 | 0.0694, 0.1653 | 0.0415, 0.0464 |
| Largest difference in peak and hole (e Å$^{-3}$) | 1.16 and −1.25 | 3.09 and −3.01 | 2.46 and −0.95 |
| $T_{min}/T_{max}$ | 0.10/0.20 | 0.06/0.17 | 0.45/1.0 |

**Table 7**
Crystallographic and data collection parameters for complexes **7**, **10** and **11**

| Complex | **7** | **10** | **11** |
|---|---|---|---|
| Empirical formula | $C_{16}H_{18}Br_2N_4Pt$ | $C_{18}H_{18}Br_2N_4Pt$ | $C_{34}H_{38}Br_3N_4PPt_2$ |
| Formula weight | 621.25 | 645.27 | 1163.56 |
| Crystal system | orthorhombic | tetragonal | orthorhombic |
| Space group | *Pbcn* | *I*$\bar{4}$2*d* | *Pbca* |
| Z | 4 | 8 | 8 |
| *a* (Å) | 10.546(2) | 16.327(2) | 16.656(3) |
| *b* (Å) | 9.220(2) | 16.327(2) | 17.956(4) |
| *c* (Å) | 18.391(3) | 13.839(2) | 24.306(4) |
| $\alpha$ (°) | 90 | 90 | 90 |
| $\beta$ (°) | 90 | 90 | 90 |
| $\gamma$ (°) | 90 | 90 | 90 |
| *V* (Å$^3$) | 1788.1(6) | 3689.4(9) | 7270(2) |
| $\rho$ (g cm$^{-3}$) | 2.308 | 2.323 | 2.126 |
| μ (Mo K$\alpha$) (mm$^{-1}$) | 12.32 | 11.95 | 11.06 |
| *F*(000) | 1160 | 2432 | 4368 |
| Scan range (°) | 2.93 < $\theta$ < 25.89 | 1.93 < $\theta$ < 26.02 | 2.07 < $\theta$ < 26.05 |
| Reciprocal lattice segments *h*, *k*, *l* | −12 → 12 | −19 → 19 | −20 → 20 |
| | −11 → 11 | −19 → 17 | −22 → 22 |
| | −20 → 22 | −17 → 17 | −29 → 28 |
| Reflections collected | 10414 | 10073 | 49385 |
| Reflections independent | 1704 | 1794 | 7119 |
| Observed reflections | 1299 | 1594 | 4860 |
| Data/restraints/parameters | 1704/0/106 | 1794/0/116 | 7119/0/402 |
| Goodness-of-fit on $F^2$ | 1.044 | 0.960 | 0.947 |
| $R_1$, $wR_2$ [$I > 2\sigma(I)$] | 0.0468, 0.1169 | 0.0254, 0.0450 | 0.0496, 0.1104 |
| $R_1$, $wR_2$ (all data) | 0.0611, 0.1253 | 0.0329, 0.0466 | 0.780, 0.1204 |
| Largest difference in peak and hole (e Å$^{-3}$) | 1.80 and −3.68 | 0.46 and −0.55 | 1.72 and −2.12 |
| $T_{min}/T_{max}$ | 0.05/0.11 | 0.15/0.28 | 0.14/0.26 |

## Acknowledgements

The authors acknowledge Dr. T. Müller for thermogravimetric analysis, Merck for gifts of chemicals and Deutsche Forschungsgemeinschaft for financial support.

## Appendix A. Supplementary material

CCDC 676492, 676493, 676494, 676495, 676496 and 676497 contain the supplementary crystallographic data for **2**, **5, 6, 7**, **10** and **11**. These data can be obtained free of charge from The Cambridge Crystallographic Data Centre via www.ccdc.cam.ac.uk/data_request/cif. Supplementary data associated with this article can be found, in the online version, at doi:10.1016/j.ica.2008.06.025.

## References

[1] [a] M.D. Hall, H.R. Mellor, R. Callaghan, T.W. Hambley, J. Med. Chem. 50 (15) (2007) 3403;
[b] L.R. Kelland, G. Abel, M.J. McKeage, M. Jones, P.M. Goddard, M. Valenti, B.A. Murrer, K.R. Harrap, Cancer Res. 53 (1993) 2581;
[c] R. Lindner, G.N. Kaluđerović, R. Paschke, Ch. Wagner, D. Steinborn, Polyhedron 27 (2007) 914;
[d] G.N. Kaluđerović, D. Miljković, M. Momcilović, V.M. Djinović, M.M. Stojković, T.J. Sabor, V. Trajković, Int. J. Cancer 116 (2005) 479.
[2] J.R. Hall, G.A. Swile, J. Organomet. Chem. 56 (1973) 419.
[3] T.G. Appleton, C.J. D'Alton, J.R. Hall, M.T. Mathieson, M.A. Williams, Can. J. Chem. 74 (1996) 2008.
[4] J.R. Hall, G.A. Swile, Aust. J. Chem. 24 (1971) 423.
[5] R. Contreas, M. Valderrama, C. Beroggi, D. Boys, Polyhedron 20 (2001) 3127.
[6] G.N. Kaluderović, H. Schmidt, Ch. Wagner, D. Steinborn, Acta Crystallogr., Sect. E 63 (8) (2007) m1985.
[7] [a] E.W. Abel, M.A. Beckett, P.A. Bates, M.B. Hursthouse, J. Organomet. Chem. 325 (1987) 261;
[b] A.T. Hutton, B. Shabanzadeh, B.L. Shaw, J. Chem. Soc., Chem. Commun. (1982) 1345;
[c] C.R. Baar, G.S. Hill, J.J. Vittal, R.J. Puddephatt, Organometallics 17 (1998) 32;
[d] E.W. Abel, A.R. Khan, K. Kite, K.G. Orrell, V. Šik, T.S. Cameron, R. Cordes, J. Chem. Soc., Chem. Commun. (1979) 713;
[e] W. Massa, G. Baum, B.-S. Seo, J. Lorberth, J. Organomet. Chem. 352 (1988) 415;
[f] P.V. Bernhardt, C. Gallego, M. Martinez, Organometallics 19 (2000) 4862.
[8] R. Contreras, M. Valderrama, E.M. Orellana, D. Boys, D. Carmona, L.A. Oro, M.P. Lamata, J. Ferrer, J. Organomet. Chem. 606 (2000) 197.
[9] D. Carmona, F.J. Lahoz, R. Atencio, A.J. Edwards, L.A. Oro, M.P. Lamata, M. Esteban, S. Troimenko, Inorg. Chem. 35 (1996) 2549.
[10] D. Carmona, J. Ferrer, F.J. Lahoz, L.A. Oro, J. Reyes, M. Esteban, J. Chem. Soc., Dalton Trans. (1991) 2811.
[11] G.W. Bushnell, D.O.K. Fjeldsted, S.R. Stobart, M.J. Zaworotko, S.A.R. Knox, K.A. Macpherson, Organometallics 4 (1985) 1107.
[12] K.A. Beveridge, G.W. Bushnell, S.R. Stobart, J.L. Atwood, M.J. Zaworotko, Organometallics 2 (1983) 1447.
[13] D. Carmona, A. Mendoza, J. Ferrer, F.J. Lahoz, L.A. Oro, J. Organomet. Chem. 431 (1992) 87.
[14] P. Beagley, E.J. Starr, J. Basca, J.R. Moss, A.T. Hutton, J. Organomet. Chem. 645 (2002) 206.
[15] E.C. Alyea, A. Somogyvari, Magn. Reson. Chem. 24 (1986) 357.
[16] S. Hietkamp, D.J. Stufkens, K. Vrieze, J. Orgnomet. Chem. 169 (1979) 107.
[17] S. Lanza, Inorg. Chim. Acta 75 (1983) 131.
[18] J.D. Scott, R.J. Puddephatt, Organometallics 5 (1986) 1538.
[19] M. Bochmann, G. Wilkinson, G.B. Young, J. Chem. Soc., Dalton Trans. (1980) 1879.
[20] [a] H.C. Clark, G. Ferguson, V.K. Jain, M. Parvez, Organometallics 2 (1983) 806;
[b] R.J. Klingler, J.C. Huffman, J.K. Kochi, J. Am. Chem. Soc. 104 (1982) 2147;
[c] J.T. Burton, R.J. Puddephatt, N.L. Jones, J.A. Ibers, Organometallics 2 (11) (1983) 1487;
[d] R.P. Hughes, J.T. Sweetser, M.D. Tawa, A. Williamson, C.D. Incarvito, B. Rhatigan, A.L. Rheingold, G. Rossi, Organometallics 20 (2001) 3800;
[e] A. Canty, R.T. Honeyman, B.W. Skelton, A.H. White, J. Organomet. Chem. 396 (1990) 105;
[f] K. Hindmarsch, D.A. House, M.M. Turnbull, Inorg. Chim. Acta 257 (1997) 11.
[21] Cambridge Structural Database (CSD), University Chemical Laboratory, Cambridge, 2006.
[22] J.E. Huheey, E.A. Keiter, R.L. Keiter, Inorganic Chemistry – Principles of Structure and Reactivity, 4th ed., HarperCollins College Publishers, 1993.
[23] L. Brammer, E.A. Burton, P. Sherwood, Cryst. Growth Des. 1 (2001) 277.
[24] C. Janiak, J. Chem. Soc., Dalton Trans. (2000) 3885.
[25] R.J. Crutchley, A.B.P. Lever, Inorg. Chem. 21 (1982) 2276.
[26] [a] IPDS – Software Package, Stoe & Cie, 1999;
[b] X-RED32, Empirical Absorption Correction, Stoe & Cie, 1996;
[c] SCALE3 ABSPACK: Empirical Absorption Correction, CRYSALIS – Software Package, Oxford Diffraction Ltd., 2006.
[27] [a] G.M. Sheldrick, SHELXS-97, Program for Crystal Structure Solution Göttingen, 1997;
[b] G.M. Sheldrick, SHELXL-97, Program for the Refinement of Crystal Structures, Göttingen, 1997.
[28] K. Branderburg, Diamond, Release 2, Crystal Impact GbR, Bonn, 1997.